HHS Public Access

Author manuscript

Biochem Biophys Res Commun. Author manuscript; available in PMC 2019 February 05.

Published in final edited form as:

Biochem Biophys Res Commun. 2018 February 05; 496(2): 568–574. doi:10.1016/j.bbrc.2017.11.192.

A new genetically engineered mouse model of choroid plexus carcinoma

Salsabiel El Nagar[(1)], **Frederique Zindy**[(2)], **Charlotte Moens**[(1)], **Luc Martin**[(1)], **Damien Plassard**[(3)], **Martine F. Roussel**[(2)], **Thomas Lamonerie**[(1)], and **Nathalie Billon**[(1),#]

[(1)]Université Côte d'Azur, CNRS, Inserm, iBV, Nice, France

[(2)]Department of Tumor Cell Biology, St. Jude Children's Research Hospital, 262 Danny Thomas Place, Memphis, TN 38105, USA

[(3)]Plateforme GenomEast, IGBMC, Illkirch, France

Abstract

Choroid plexus carcinomas (CPCs) are highly malignant brain tumours predominantly found in children and associated to poor prognosis. Improved therapy for these cancers would benefit from the generation of animal models. Here we have created a novel mouse CPC model by expressing a stabilised form of c-Myc (MycT58A) and inactivating Trp53 in the choroid plexus of newborn mice. This induced aberrant proliferation of choroid plexus epithelial cells, leading to aggressive tumour development and death within 150 days. Choroid plexus tumours occurred with a complete penetrance in all brain ventricles, with prevalence in the lateral and fourth ventricles. Histological and cellular analysis indicated that these tumours were CPCs resembling their human counterparts. Comparison of gene expression profiles of CPCs and non-neoplastic tissues revealed profound alterations in cell cycle regulation and DNA damage responses, suggesting that dysregulation of cell division and DNA checkpoint pathways may represent key vulnerabilities. This novel animal model of CPC provides an invaluable tool to elucidate the mechanism of CPC formation and to develop successful therapies against this devastating paediatric cancer.

Keywords

Choroid plexus carcinoma; mouse model; Myc; Trp53; Otx2; paediatric cancer

Introduction

Choroid plexus tumours account for up to 20% of intracranial brain tumours in children under one year of age. They are classified into three histological categories - choroid plexus papillomas (CPPs), atypical choroid plexus papillomas (ACPPs) and choroid plexus carcinomas (CPCs). While CPPs and ACPPs are relatively benign, CPCs are extremely

[#]corresponding author (billon@unice.fr).

aggressive (World Health Organization [WHO] grade III) with a 5-year survival rate of approximately 40%. Genome-wide analysis of large cohorts of paediatric choroid plexus tumours has revealed that this prognostic heterogeneity is reflected at the molecular level, since molecular signatures of CPCs strongly differ from those of CPPs/aCPPs, which might represent a single-tumour entity [1,2,3].

CPCs derive from the choroid plexus (CP), a secretory epithelium that produces cerebrospinal fluid (CSF) in each brain ventricle [4]. CPCs occur predominantly in the lateral and fourth ventricles and less often in the third ventricle or at multiple sites [5,6]. These tumours have been associated with obstruction of the CSF pathways and, potentially, overproduction of CSF, leading to hydrocephalus and increased intracranial pressure.

CPCs are characterized by numerous large chromosomal additions and deletions and very few focal alterations complicating the identification of the oncogenes and suppressor genes responsible for their pathogenesis [6,7,8]. CPCs were initially found in transgenic mice expressing SV40 T antigen, suggesting that alteration of Trp53 and/or the retinoblastoma (Rb) function might be involved [9,10]. Subsequent studies showed that Rb inactivation is required for tumour initiation, while p53 predominantly affects apoptosis of tumour cells once the lesions are formed [11]. In humans, CPC is associated with Li-Fraumeni syndrome, a familial cancer associated to r germline mutations, and with somatic *TP53* mutations, that all display increased genetic instability confirming the crucial role of TP53 alterations in this disease [1,2].

To narrow down the genetic alterations that drive CPCs, Tong et al. (2015) compared chromosomal amplifications in human CPCs and in tumours derived from a mouse model harbouring loss of Pten function together with Trp53 and Rb loss. This analysis identified a group of concurrently gained oncogenes in human and mouse CPCs, TAF12, NFYC and RAD54L, which co-localised on human and mouse chromosomes 1 and 4, respectively, and were shown to be involved in tumour initiation and progression. TAF12 and NFYC regulate the epigenome and DNA metabolism, whereas RAD54L plays a central role in DNA repair, suggesting that dysregulation of DNA maintenance and/or repair is necessary for CPC formation [12].

Finally, recent examination of a large cohort of human CP tumours uncovered *c-MYC* overexpression in 43% of cases, suggesting this transcription factor could play a predominant role in CPC formation [13]. c-MYC controls many cellular functions, including cell proliferation, genome stability and cell death. It is overexpressed in various malignancies, such as medulloblastoma and glioma, and high expression of c-MYC in animal models can drive tumourigenesis [14,15]. However, c-MYC–induced tumourigenesis is restrained by its ability to activate apoptotic pathways, and has to be combined to anti-apoptotic events, such as *TP53* loss [16].

The mechanisms underlying CPC formation remain largely unknown, mostly due to the paucity of animal models reproducing the genetic alterations associated to these cancers. Here, we conditionally overexpressed *c-Myc* and deleted *Trp53* in the CP of newborn mice. This led to aberrant CP cell proliferation and to the formation of aggressive carcinoma

resembling their human counterparts, thus providing a new model to apprehend and treat these devastating paediatric cancers.

Materials and methods

Mouse breeding and injection

All mouse experiments were approved by the Animal Care and Use Committee of St. Jude Children's Research Hospital in strict accordance with NIH guidelines. *Otx2*$^{CreERT2/+}$, *Rosa*$^{MycT58A/MycT58A}$, and *Trp53*$^{fl/fl}$ mouse lines [14, 17, 18], were crossed together to obtain *Otx2*$^{CreER/+}$; *Rosa*$^{MycT58A/MycT58A}$; *Trp53*$^{fl/fl}$ animals. Tamoxifen (50μg/g of body weight, Sigma-Aldrich, Saint Louis, USA) was administrated by intraperitoneal injection (IP) during the first postnatal week (single injection at postnatal day 3 (P3), double injection at P1 and P2, triple injection at P1, P4 and P7). IP injection of 5-Ethynyl-2′-deoxyuridine (EdU) (25μg/g of body weight) was performed 1h before sacrifice.

Immunocytochemistry and histological analysis

Brain were fixed in 4% paraformaldehyde overnight at 4°C, protected in 30% PBS-sucrose and frozen in Tissue-Tek OCT at −80°C (Fisher Scientific, Waltham, MA, USA). Sections of 16 μm were cut on a Microm HM550 cryostat, mounted on SuperFrost + slides (Fisher Scientific). For coloration, sections were dehydrated overnight in ethanol-chloroform (1:1 volume) and stained with Hematoxylin and Eosin using standard methods. Images were generated on Zeiss Axio Scan.Z1 slide scanner and analysed with NDP.view2 Viewing software (Hamamatsu, Shizuoka, Japan). For immunostaining, sections were blocked 1h in PBS with 2% gelatin, 0,2% Triton and 10% donkey serum, incubated overnight at 4°C with primary antibodies, and 1h at room temperature with secondary antibodies. Primary antibodies were: goat anti-Otx2 (1:200, R&D Systems, Minneapolis, USA), rabbit anti-GFP (1:500, Abcam, Cambridge, UK), rabbit anti-Ki67 (1:100, Thermo Scientific, clone SP6), rabbit anti-Ttr (1:100, Abbiotec, San Diego, USA), mouse anti-Aqpr1 (1:200, Abcam), rabbit anti-GFAP (1:1000), goat anti-lmx1a (1:100, Santa Cruz Biotechnology, Dallas, USA). EdU was revealed using Click-it Edu Alexa Fluor 647 Imaging Kit (Invitrogen, Waltham, USA). Nuclei were counterstained with 4′,6-diamidino-2-phenylindole (DAPI, 10ug/ml, Sigma-Aldrich). Images were generated on Zeiss 710 confocal microscope.

RNA isolation, RNA sequencing and bioinformatic analysis

Tissues were triturated in TRI-Reagent (Sigma-Aldrich). Total RNA was extracted using miRNeasy Mini Kit (Qiagen, Hilden, Germany). RNA-Seq libraries were generated using TruSeq Stranded mRNA LT Sample Preparation Kit (Illumina). All samples were sequenced on the GenomEast genomic platform (IGBMC, Illkirch, France) on the flow cells HS315 in 50-length Single-Read. Reads were mapped onto the mm10 mouse genome using Tophat 2.0.10 [19] and bowtie 2–2.1.0 [20]. Quantification of gene expression was performed using HTSeq-0.6.1 with annotations from Ensembl 84 [21]. Comparisons of interest were performed using DESeq2 1.10.1 [22]. Differentially expressed genes (DEGs) were defined as those with an absolute log2 FC≥2 and an adjusted pvalue≤0.05. The functional and pathway analyses of DEGs were generated through the use of Ingenuity Pathways Analysis (IPA, Qiagen) [23].

Results

Myc activation in postnatal choroid plexus leads to choroid plexus carcinoma

To assess the effects of Myc activation combined to Trp53 ablation in postnatal choroid plexus, we crossed mice harbouring Cre-inducible alleles of a stabilised form of c-Myc (MycT58A) [14] and Cre-deletable alleles of *Trp53* (*Trp53*^{flox}) [17,24] with mice expressing tamoxifen-inducible Cre recombinase in the CP (*Otx2*^{CreER}) [18], creating *Otx2*$^{CreER/+}$; *Rosa*$^{MycT58A/MycT58A}$; *Trp53*$^{fl/fl}$ animals (Fig. 1A). Otx2 was chosen to drive Cre expression because it is strongly expressed in all CP epithelial cells of the lateral, third, and fourth brain ventricles, allowing efficient postnatal recombination in these tissues (Sup. Fig. 1).

We induced concomitant expression of c-MycT58A and Trp53 ablation in *Otx2*$^{CreER/+}$; *Rosa*$^{MycT58A/MycT58A}$; *Trp53*$^{fl/fl}$ animals by single, or multiple injection of tamoxifen during the first postnatal week. This resulted in aggressive tumour formation with a 100% penetrance. After 100 days, half of the treated mice had succumbed from hydrocephalus, and all of them had died by 150 days (Fig. 1B). Pathological analysis revealed the presence of CPCs in all cases, mainly located at the level of the 4th ventricle and lateral ventricles, and less frequently in the third ventricle (Table 1). Repeating tamoxifen induction during the first postnatal week had no incidence on the frequency of tumour or the survival rate of *Otx2*$^{CreER/+}$; *Rosa*$^{MycT58A/MycT58A}$; *Trp53*$^{fl/fl}$ animals, confirming that efficient recombination could be obtained via a single injection.

Histology of the tumours formed in *Otx2*$^{CreER/+}$; *Rosa*$^{MycT58A/MycT58A}$; *Trp53*$^{fl/fl}$ mice revealed typical features of human choroid plexus carcinoma, such as pronounced enlargement of the tissues, increased cellularity, nuclear pleomorphism, and high vascularization (Fig. 1C). Mouse CPCs expressed the LIM homeobox transcription factor 1 alpha (Lmx1a), a CP marker, indicating that they kept their lineage identity. They also expressed the differentiation markers aquaporin 1 (Aqp1) and transthyretin (Ttr), although to a lower extent than normal tissues, suggesting that Myc-induced carcinogenesis might interfere with their differentiation. Accordingly, sustained mitotic activity could be revealed by the many cells expressing the Ki-67 proliferation marker. By contrast, Glial fibrillary acidic protein (Gfap), which displays variable expression in CPCs, was undetectable (Fig. 1D) [25].

To assess the early effects of MycT58A induction and Trp53 ablation on cell proliferation, we measured EdU incorporation in choroid plexus at P9 (Fig. 1E,F). While at this stage, the mean proliferation index in controls oscillated between 0.5% in the fourth ventricle, to 2% in the third and lateral ventricles, this index was increased by 2.5 to 10-fold in the CP of aged-matched, recombined *Otx2*$^{CreER/+}$; *Rosa*$^{MycT58A/MycT58A}$; *Trp53*$^{fl/fl}$ regardless of their location.

Therefore, Myc activation and Trp53 ablation in postnatal *Otx2*$^{CreER/+}$; *Rosa*$^{MycT58A/MycT58A}$; *Trp53*$^{fl/fl}$ mice caused aberrant proliferation, transforming CP into aggressive CPC tumours.

Comprehensive gene expression profiling reveals abnormal cell division and DNA checkpoints pathways in CPCs

To identify the early signals that drive CPC tumourigenesis, we compared transcriptional profiles of control CP and tumours at P9, shortly after MycT58A induction and Trp53 ablation. Tumours and CPCs clustered apart in principal component analysis, pinpointing divergent molecular profiles (Sup. Fig. 2). Tumour cells displayed 191 differentially expressed genes (DEGs), of which 145 were upregulated and 46 were downregulated (absolute log2 fold change ≥2 and adj. p-value < 0.05) (Sup. Fig. 2, Sup. Table 1). Inspection of the “diseases and functions” gene ontology (GO) terms enriched in DEGs disclosed a strong association to “Cancer, Organismal Injury and Abnormalities”, with similarities to other forms of epithelial cancers such as lung, pancreatic, hepatic, gastrointestinal, and uterine carcinoma. “DNA replication, recombination and repair”, “chromosomal instability”, “cell cycle”, and “proliferation of cancer cells” also appeared as CPC-enriched categories (Fig. 2A, Sup. Table 1).

We next assigned DEGs to pathways using Ingenuity Pathway Analysis (IPA, Qiagen). This approach identified several signalling and metabolic cascades involved in cell division, DNA damage-induced cell cycle checkpoint regulation, and DNA maintenance and/or repair, as significantly over-represented in tumour cells (Fig. 2B). Inspection of individual members of these pathways confirmed that many pro-mitotic cell cycle regulators, such as cyclin B1, cyclin B2, cyclin A1, cdc25, and cdk1, were strongly overexpressed in CPCs, suggesting that tumour cells were actively dividing (Sup. Table 1). This perfectly matched with the enhanced EdU incorporation observed in P9 CP cells of induced $Otx2^{CreER/+}$; $Rosa^{MycT58A/MycT58A}$; $Trp53^{fl/fl}$ mice (Fig. 1E,F).

This analysis highlighted genomic instability and DNA damage responses in CPCs. The tumour suppressor Brca1, which plays a crucial role in DNA repair and cell cycle checkpoints activation upon DNA damage, was strongly upregulated in CPCs (Sup. Table 1) [26]. We also noticed significant upregulation of the Aurora kinase (AurA) and the Polo-like kinase 1 (Plk1), which enhance the progression of many cancers by promoting mitotic abnormality and genetic instability [27].

Finally, we compared the transcriptome signature of $Otx2^{CreER/+}$; $Rosa^{MycT58A/MycT58A}$; $Trp53^{fl/fl}$ CPCs to other mouse models of choroid plexus tumours. To do so, we first overlapped the list of transcripts differentially expressed in our model with those found modulated in CPC samples derived from *Trp53/Rb/Pten* null mice (Tong et al 2015). We found that the *Trp53/Rb/Pten*, model shared 115 out of 191 (60%) of the $Otx2^{CreER/+}$; $Rosa^{MycT58A/MycT58A}$; $Trp53^{fl/fl}$ DEGs, emphasizing their striking resemblances (Fig. 2D). Interrogating the list of transcripts commonly modulated in these two models using IPA functional analysis revealed marked enrichment and regulation of signalling pathways involved in cell proliferation and DNA damage-responses, implicating that modification of these cascades represent core features of CPC tumourigenesis (Fig. 2E).

DISCUSSION

One major barrier to the successful implementation of efficient therapy for many childhood cancers is the lack of appropriate preclinical models. Here we describe the generation of a novel mice model of choroid plexus carcinoma, offering a unique opportunity to identify tumour vulnerabilities and potential therapeutic targets.

$Otx2^{CreER/+}$; $Rosa^{MycT58A/MycT58A}$; $Trp53^{fl/fl}$ mice, a bona fide model of CPCs

Human CPCs are often associated with *TP53* mutation [1,2] and *c-MYC* overexpression [13]. The model we generated here combines these two alterations by expressing a stabilised form of c-Myc (T58A) directly into the CP of newborn mice through an *Otx2*-driven inducible Cre recombinase, in a *Trp53* null background. This led to aberrant proliferation of CP epithelial cells and formation of aggressive CPCs in 100% of the mice. Moreover, the present model recapitulates many features of human CPCs, such as hydrocephalus, pleomorphic epithelioid cytology, increased mitotic figures, and preponderance of tumours in the lateral and the fourth ventricles [25]. It therefore provides an invaluable *in vivo* system to decipher the mechanisms that contribute to cancer initiation and progression of this tumor subgroup and to identify novel therapeutics via preclinical testing.

Tumour tropism for choroid plexus

Dysregulation of c-MYC is found in several paediatric brain tumours, such as Group3 medulloblastoma (MBG3), which also have a dismal prognostic. Novel mouse models of MBG3 were developed through orthotopic transplantation of c-Myc overexpressing cerebellar progenitors [28,29] or *in utero* electroporation of c-Myc in different cell populations of the 4^{th} ventricle in the absence of Trp53 loss of function [30]. Interestingly, a significant part of the mice electroporated to express c-Myc in Atoh1+ precursors developed CPCs instead of medulloblastoma, due to expression of Atoh1 in a fraction of CP cells. This demonstrates that the same oncogenic insult can drive different tumour types depending on the nature of its cell-of-origin. Here, MycT58A expression was driven by the *Otx2*-CreER line in newborn mice. At this stage, Otx2 is strongly expressed in all CP, but also in Atoh1+ granule cell precursors (GCPs) of the developing cerebellum. Intriguingly, these mice always develop CPCs, but never form medulloblastoma. Tumour tropism was not due to restricted recombination in CP, since active Cre was easily detected in the postnatal cerebellum. Furthermore, the same *Otx2-CreER* line can drive constitutive expression of an activated form of Smoothened in postnatal GCP, leading to the formation of SHH medulloblastoma (El Nagar *et al.*, submitted). However, the selective development of CPCs in our model might reflect different sensitivity of GCP versus CP cells to c-Myc activation. Here, MycT58A is expressed under the control of the relatively weak Rosa26 promoter. Such moderate expression appears sufficient to induce tumorigenesis in CP epithelial cells, but may not be high enough to induce MBG3 formation in GCP. In line with this hypothesis, c-Myc-driven medulloblastoma described by Kawauchi *et al.* (2017) required the strong CAG promoter to achieve high c-Myc expression. The kinase and phosphatase content of targeted cells might also influence c-Myc half-life. c-Myc phosphorylation on serine 62 by ERK, opposed by PP2A, enhances its stability, while threonine 58 phosphorylation enhances its degradation [31]. As MycT58A variant can only be phosphorylated on serine 62, its

stability mostly relies on the balance between ERK and PP2A activity. Contrasted ERK and PP2A activity in CP cells and in GCPs could differentially influence c-Myc stability. Further investigation will be required to understand why *Otx2*$^{CreER/+}$; *Rosa*$^{MycT58A/MycT58A}$; *Trp53*$^{fl/fl}$ mice exclusively develop CPCs. Nevertheless, the exclusion of other neoplastic lesions in this model makes it ideal for preclinical testing and for successful implementation of individualized therapy against MYC-induced CPCs.

Mechanisms of c-Myc-induced choroid plexus carcinoma formation

c-MYC contributes to tumourigenesis by enhancing cell proliferation and genomic instability (Pelengaris et al., 2002). Myc overexpression leads to aberrant activation and premature firing of several origins of replication, causing replication stress (RS) (Srinivasan, Dominguez-Sola, Wang, Hyrien and Gautier, 2013). RS plays a prominent role in oncogenesis, and constitutes a feature of pre-cancerous and cancerous cells [32]. Here, large-scale gene expression analysis shortly after transformation revealed marked increase in the expression of many pro-mitotic and DNA damage/repair factors in CPCs, indicating that tumour cells might bypass DNA-damage-induced cell cycle checkpoints and accumulate genomic alterations. These findings suggest that, as in other types of cancers, c-Myc might accelerate CPC progression by promoting RS and genetic instability in CP cells [33]. Other murine models of CPCs, as well as primary human CPCs, were also shown to exhibit genomic instability and aberrant DNA metabolism, indicating that deregulation of DNA maintenance and/or repair may represent key features for CPC tumourigenesis [12]. The genome-wide molecular characterisation of the *Otx2*$^{CreER/+}$; *Rosa*$^{MycT58A/MycT58A}$; *Trp53*$^{fl/fl}$ model should help identifying the precise mechanisms by which c-Myc expression and Trp53 ablation contribute to the development of aggressive tumours in neonates. Interestingly, pharmacological inhibition of AurA and Plk1, two kinases strongly upregulated in our model, has recently gathered great interest as potential therapy for treating paediatric cancers [34].

It is therefore expected that the new animal model we created here can be used not only to elucidate the basic biology of CPCs, but can also serve as a platform for discovering tumour vulnerabilities and validating potential therapeutic targets.

Supplementary Material

Refer to Web version on PubMed Central for supplementary material.

Acknowledgments

S.E.N. received fellowships from the Ligue Nationale Contre le Cancer. This work was supported by grants from Cancéropôle PACA, and in part by National Cancer Institute (to MFR) and the American Lebanese Syrian Associated Charities of St. Jude Children's Research Hospital. We thank S. Robinson and D. Farmer for mouse genotyping, and R. Sears and A. Berns for providing *Rosa*^{MycT58A}, and *Trp53*^{fl} mouse lines.

References

1. Merino DM, Shlien A, Villani A, Pienkowska M, Mack S, Ramaswamy V, Shih D, Tatevossian R, Novokmet A, Choufani S, Dvir R, Ben-Arush M, Harris BT, Hwang EI, Lulla R, Pfister SM, Achatz MI, Jabado N, Finlay JL, Weksberg R, Bouffet E, Hawkins C, Taylor MD, Tabori U, Ellison DW,

Gilbertson RJ, Malkin D. Molecular characterization of choroid plexus tumors reveals novel clinically relevant subgroups. Clin Cancer Res. 2015; 21:184–192. [PubMed: 25336695]

2. Tabori U, Shlien A, Baskin B, Levitt S, Ray P, Alon N, Hawkins C, Bouffet E, Pienkowska M, Lafay-Cousin L, Gozali A, Zhukova N, Shane L, Gonzalez I, Finlay J, Malkin D. TP53 alterations determine clinical subgroups and survival of patients with choroid plexus tumors. J Clin Oncol. 2010; 28:1995–2001. [PubMed: 20308654]
3. Li L, Grausam KB, Wang J, Lun MP, Ohli J, Lidov HG, Calicchio ML, Zeng E, Salisbury JL, Wechsler-Reya RJ, Lehtinen MK, Schuller U, Zhao H. Sonic Hedgehog promotes proliferation of Notch-dependent monociliated choroid plexus tumour cells. Nat Cell Biol. 2016; 18:418–430. [PubMed: 26999738]
4. Lun MP, Johnson MB, Broadbelt KG, Watanabe M, Kang YJ, Chau KF, Springel MW, Malesz A, Sousa AM, Pletikos M, Adelita T, Calicchio ML, Zhang Y, Holtzman MJ, Lidov HG, Sestan N, Steen H, Monuki ES, Lehtinen MK. Spatially heterogeneous choroid plexus transcriptomes encode positional identity and contribute to regional CSF production. J Neurosci. 2015; 35:4903–4916. [PubMed: 25810521]
5. Rickert CH, Paulus W. Tumors of the choroid plexus. Microsc Res Tech. 2001; 52:104–111. [PubMed: 11135453]
6. Paulus W, Brander S. Choroid plexus tumors. In: The 2007 WHO classification of tumours of the central nervous system (Louis, D. N. et al.). Acta Neuropathol. 2007; 114:97–109. [PubMed: 17618441]
7. Ruland V, Hartung S, Kordes U, Wolff JE, Paulus W, Hasselblatt M. Choroid plexus carcinomas are characterized by complex chromosomal alterations related to patient age and prognosis. Genes Chromosomes Cancer. 2014; 53:373–380. [PubMed: 24478045]
8. Rickert CH, Wiestler OD, Paulus W. Chromosomal imbalances in choroid plexus tumors. Am J Pathol. 2002; 160:1105–1113. [PubMed: 11891207]
9. Saenz Robles MT, Symonds H, Chen J, Van Dyke T. Induction versus progression of brain tumor development: differential functions for the pRB- and p53-targeting domains of simian virus 40 T antigen. Mol Cell Biol. 1994; 14:2686–2698. [PubMed: 8139568]
10. Brinster RL, Chen HY, Messing A, van Dyke T, Levine AJ, Palmiter RD. Transgenic mice harboring SV40 T-antigen genes develop characteristic brain tumors. Cell. 1984; 37:367–379. [PubMed: 6327063]
11. Symonds H, Krall L, Remington L, Saenz Robles M, Jacks T, Van Dyke T. p53-dependent apoptosis in vivo: impact of p53 inactivation on tumorigenesis. Cold Spring Harb Symp Quant Biol. 1994; 59:247–257. [PubMed: 7587076]
12. Tong Y, Merino D, Nimmervoll B, Gupta K, Wang YD, Finkelstein D, Dalton J, Ellison DW, Ma X, Zhang J, Malkin D, Gilbertson RJ. Cross-Species Genomics Identifies TAF12, NFYC, and RAD54L as Choroid Plexus Carcinoma Oncogenes. Cancer Cell. 2015; 27:712–727. [PubMed: 25965574]
13. Merve A, Acquati S, Hoeck J, Jeyapalan J, Behrens A, Marino S. TMOD-01. CMYC OVEREXPRESSION INDUCES CHOROID PLEXUS TUMOURS THROUGH MODULATION OF INFLAMMATORY PATHWAYS. Neuro-Oncology. 2017; 19:iv48–iv48.
14. Wang X, Cunningham M, Zhang X, Tokarz S, Laraway B, Troxell M, Sears RC. Phosphorylation regulates c-Myc's oncogenic activity in the mammary gland. Cancer Res. 2011; 71:925–936. [PubMed: 21266350]
15. Pelengaris S, Khan M, Evan G. c-MYC: more than just a matter of life and death. Nat Rev Cancer. 2002; 2:764–776. [PubMed: 12360279]
16. Momota H, Shih AH, Edgar MA, Holland EC. c-Myc and beta-catenin cooperate with loss of p53 to generate multiple members of the primitive neuroectodermal tumor family in mice. Oncogene. 2008; 27:4392–4401. [PubMed: 18372915]
17. Marino S, Vooijs M, van Der Gulden H, Jonkers J, Berns A. Induction of medulloblastomas in p53-null mutant mice by somatic inactivation of Rb in the external granular layer cells of the cerebellum. Genes Dev. 2000; 14:994–1004. [PubMed: 10783170]
18. Fossat N, Chatelain G, Brun G, Lamonerie T. Temporal and spatial delineation of mouse Otx2 functions by conditional self-knockout. EMBO Rep. 2006; 7:824–830. [PubMed: 16845372]

19. Kim D, Pertea G, Trapnell C, Pimentel H, Kelley R, Salzberg SL. TopHat2: accurate alignment of transcriptomes in the presence of insertions, deletions and gene fusions. Genome Biol. 2013; 14:R36. [PubMed: 23618408]
20. Langmead B, Trapnell C, Pop M, Salzberg SL. Ultrafast and memory-efficient alignment of short DNA sequences to the human genome. Genome Biol. 2009; 10:R25. [PubMed: 19261174]
21. Anders S, Pyl PT, Huber W. HTSeq--a Python framework to work with high-throughput sequencing data. Bioinformatics. 2015; 31:166–169. [PubMed: 25260700]
22. Love MI, Huber W, Anders S. Moderated estimation of fold change and dispersion for RNA-seq data with DESeq2. Genome Biol. 2014; 15:550. [PubMed: 25516281]
23. Kramer A, Green J, Pollard J Jr, Tugendreich S. Causal analysis approaches in Ingenuity Pathway Analysis. Bioinformatics. 2014; 30:523–530. [PubMed: 24336805]
24. Donehower LA, Harvey M, Slagle BL, McArthur MJ, Montgomery CA Jr, Butel JS, Bradley A. Mice deficient for p53 are developmentally normal but susceptible to spontaneous tumours. Nature. 1992; 356:215–221. [PubMed: 1552940]
25. Gopal P, Parker JR, Debski R, Parker JC Jr. Choroid plexus carcinoma. Arch Pathol Lab Med. 2008; 132:1350–1354. [PubMed: 18684041]
26. Wu J, Lu LY, Yu X. The role of BRCA1 in DNA damage response. Protein Cell. 2010; 1:117–123. [PubMed: 21203981]
27. Fu J, Bian M, Jiang Q, Zhang C. Roles of Aurora kinases in mitosis and tumorigenesis. Mol Cancer Res. 2007; 5:1–10. [PubMed: 17259342]
28. Kawauchi D, Robinson G, Uziel T, Gibson P, Rehg J, Gao C, Finkelstein D, Qu C, Pounds S, Ellison DW, Gilbertson RJ, Roussel MF. A mouse model of the most aggressive subgroup of human medulloblastoma. Cancer Cell. 2012; 21:168–180. [PubMed: 22340591]
29. Hanaford AR, Archer TC, Price A, Kahlert UD, Maciaczyk J, Nikkhah G, Kim JW, Ehrenberger T, Clemons PA, Dancik V, Seashore-Ludlow B, Viswanathan V, Stewart ML, Rees MG, Shamji A, Schreiber S, Fraenkel E, Pomeroy SL, Mesirov JP, Tamayo P, Eberhart CG, Raabe EH. DiSCoVERing Innovative Therapies for Rare Tumors: Combining Genetically Accurate Disease Models with In Silico Analysis to Identify Novel Therapeutic Targets. Clin Cancer Res. 2016; 22:3903–3914. [PubMed: 27012813]
30. Kawauchi D, Ogg RJ, Liu L, Shih DJH, Finkelstein D, Murphy BL, Rehg JE, Korshunov A, Calabrese C, Zindy F, Phoenix T, Kawaguchi Y, Gronych J, Gilbertson RJ, Lichter P, Gajjar A, Kool M, Northcott PA, Pfister SM, Roussel MF. Novel MYC-driven medulloblastoma models from multiple embryonic cerebellar cells. Oncogene. 2017; 36:5231–5242. [PubMed: 28504719]
31. Yeh E, Cunningham M, Arnold H, Chasse D, Monteith T, Ivaldi G, Hahn WC, Stukenberg PT, Shenolikar S, Uchida T, Counter CM, Nevins JR, Means AR, Sears R. A signalling pathway controlling c-Myc degradation that impacts oncogenic transformation of human cells. Nat Cell Biol. 2004; 6:308–318. [PubMed: 15048125]
32. Gaillard H, Garcia-Muse T, Aguilera A. Replication stress and cancer. Nat Rev Cancer. 2015; 15:276–289. [PubMed: 25907220]
33. Vafa O, Wade M, Kern S, Beeche M, Pandita TK, Hampton GM, Wahl GM. c-Myc can induce DNA damage, increase reactive oxygen species, and mitigate p53 function: a mechanism for oncogene-induced genetic instability. Mol Cell. 2002; 9:1031–1044. [PubMed: 12049739]
34. Pezuk JA, Valera ET, Brassesco MS. PLK1 Inhibition: Prospective Role for the Treatment of Pediatric Tumors. Curr Drug Targets. 2016; 17:1661–1672. [PubMed: 26302797]

Highlights

- Description of a new mouse model for choroid plexus carcinoma (CPC)
- CPC arose upon MycT58A expression and Trp53 deletion in 100% of newborn mice
- This model recapitulates human disease
- Genome-wide analysis revealed genomic instability as a hallmark of CPC
- A new preclinical model to test novel drugs against Myc-induced CPC

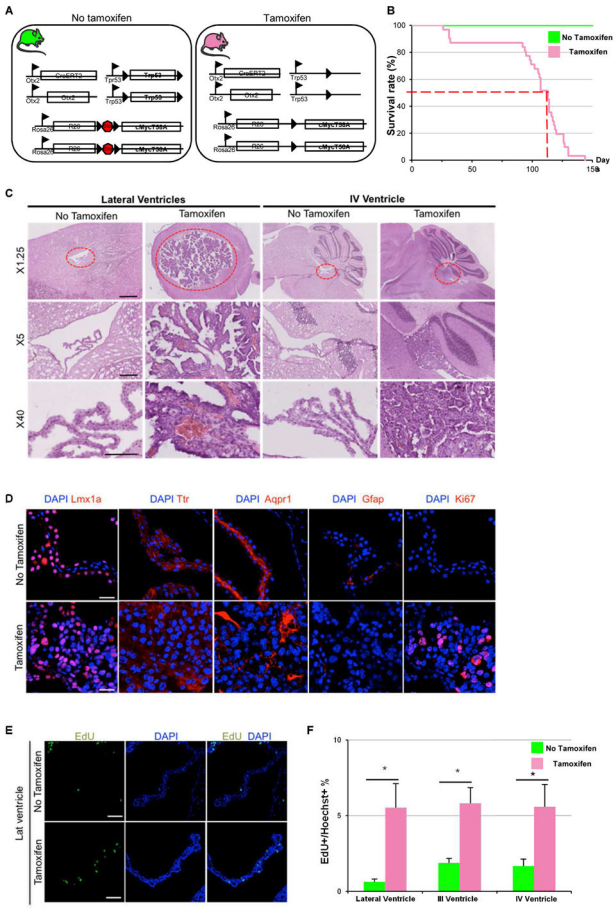

Figure 1. A new genetically-engineered mouse model of choroid plexus carcinoma

(A) Schematics of *Otx2*$^{CreER/+}$; *Rosa*$^{MycT58A/MycT58A}$; *Trp53*$^{fl/fl}$ mice. Tamoxifen injection of newborns leads to concomitant expression of c-MycT58A and Trp53 ablation in Otx2-expressing CP cells. (B) Kaplan-Meyer survival curves of control (green) and tamoxifen-injected (pink) mice. (C) Hematoxylin/Eosin staining of the adult lateral and fourth ventricles in control or P3 tamoxifen-injected mice. Choroid plexus are (D) Immuno-staining of Lmx1a (red), Transthyretin (Ttr), Aquaporin1 (Aqp1), Gfap and Ki67 in representative normal or neoplastic lateral ventricle CP from control or tamoxifen-injected adult mice. (E, D) Quantification of EdU positive cells in the CP of lateral, third and fourth ventricle at P9. Nuclei were counterstained with DAPI (blue). P= postnatal. CPCs= choroid plexus carcinomas; Scale bar: 1 mm (C, 1.25X), 250 μm (C, 5X), 100 μm (C, 40X) and 25 μm (D,E). Results are presented as the mean ± SEM. *p<0.05 (two-tailed Student's t-test).

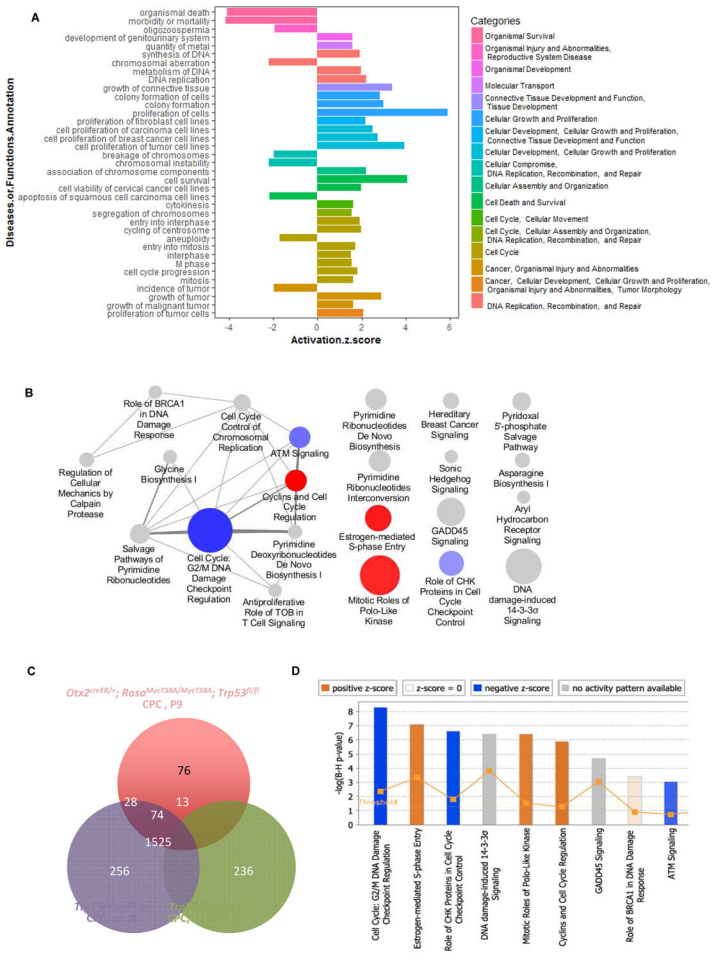

Figure 2. Molecular characterisation of *Otx2*$^{CreER/+}$; *Rosa*$^{MycT58A/MycT58A}$; *Trp53*$^{fl/fl}$ CPCs by transcriptome analysis

(A) IPA Functional analysis of differentially expressed genes (DEG) in CPCs at P9 (log2 FC >=2 or <=2; and p-adjusted value < 0.05). The most enriched biological functions are highlighted with different colours and displayed upon their levels of significance (z score up to 1 and below -1). Bar color correspond to IPA diseases and functions categories. (B) IPA pathways analysis of DEGs in CPCs. The most significant canonical pathways are displayed as nodes whose size is correlated to the number of DEGs in the pathway and the color is a function of the Ingenuity activation z score (Blue = predicted negative activation; red = predicted positive activation; grey = no possible prediction, Cytoscape representation). Edge width between pathways indicates number of shared DEGs (1 to 4). (C) Meta-analysis of the transcriptomic signature of *Otx2*$^{CreER/+}$; *Rosa*$^{MycT58A/MycT58A}$; *Trp53*$^{fl/fl}$ CPCs compared to Trp53/Rb/Pten null mice CPCs. 2 sets of DEGs were derived from the Trp53/Rb/Pten model, since tumour cells were compared to either control embryonic CP, or adult CP. Overlapping of DEGs in the two models reveals marked similarities. (D) IPA pathway analysis of the genes commonly regulated in these 2 models suggesting abnormal regulation of cell division and DNA maintenance as core features of CPC tumourigenesis.

Table 1

Overview of survival rate and CPC location in *Otx2*$^{CreER/+}$; *Rosa*$^{MycT58A/MycT58A}$; *Trp53*$^{fl/fl}$ mice after single, double, or triple injection of tamoxifen.

Case	Tamoxifen	Age	CPC location
1	P3	144	4th ventricle
2	P3	26	4th ventricule
3	P3	118	3rd ventricle
4	P3	31	4th ventricule
5	P3	105	Lateral + 4th ventricles
6	P3	98	Lateral + 4th ventricles
7	P3	94	Lateral ventricule
8	P3	106	Lateral + 4th ventricles
9	P1, P2	130	Lateral + 4th ventricles
10	P1, P2	32	Lateral + 4th ventricles
11	P1, P2	107	Lateral + 4th ventricles
12	P1, P2	127	Lateral ventricle
13	P1, P2	119	4th ventricle
14	P1, P2	130	Lateral + 4th ventricles
15	P1, P2	99	Lateral + 3rd + 4th ventricles
16	P1, P2	92	Lateral ventricle
17	P1, P2	114	Lateral ventricle
18	P1, P4, P7	113	Lateral + 4th ventricles
19	P1, P4, P7	120	Lateral ventricle
20	P1, P4, P7	126	Lateral + 3rd + 4th ventricles
21	P1, P4, P7	28	4th ventricle
22	P1, P4, P7	95	Lateral ventricle
23	P1, P4, P7	102	Lateral + 4th ventricles
24	P1, P4, P7	106	Lateral ventricle